Kinetic and structural characterisation of the ubiquinol-binding site and oxygen reduction by the trypanosomal alternative oxidase

Article (Accepted Version)

Kinetic and structural characterisation of the ubiquinol-binding site and oxygen reduction by the trypanosomal alternative oxidase.

Luke Young[a], Alicia Rosell-Hidalgo[a], Daniel Ken Inaoka[b], Fei Xu[a,c], Mary Albury[a], Benjamin May[a,d], Kiyoshi Kita[e] and Anthony L. Moore[a]

[a] Biochemistry and Biomedicine, School of Life Sciences, University of Sussex, Falmer, Brighton BN1 9QG;

[b] Department of molecular infection dynamics, Shinogi Global infectious diseases division, Institute of tropical medicine (NEKKEN), Nagasaki University, Nagasaki 852-8523, Japan;

[c] Current address: Applied Biotechnology Center, Wuhan Institute of Bioengineering, Wuhan 430415, China

[d] Current address: Theradex (Europe) Ltd, 2nd Floor, The Pinnacle, Station Way, Crawley RH10 1JH

[e] School of Tropical Medicine and Global Health, Nagasaki University, Nagasaki 852-8523, Japan

Competing Interests
L.Y., B.M. and A.L.M. hold patents and financial interests in the development of phytopathogenic fungicides.

Author contributions

Luke Young, Conceptualisation, methodology, writing original draft, investigation, Formal analysis.**: Alicia Rosell-Hidalgo,** investigation, writing review and editing.: **Daniel Ken Inaoka,** Conceptualisation, writing review and editing. **: Fei Xu,** investigation, writing review and editing. **: Mary Albury,** writing review and editing, project administration.**: Benjamin May,** investigation, writing review and editing. **: Kiyoshi Kita** Conceptualisation, writing review and editing. **: Anthony L. Moore** Conceptualisation, writing review and editing, supervision, funding acquisition

Abstract

The alternative oxidase (AOX) is a monotopic di-iron carboxylate protein which acts as a terminal respiratory chain oxidase in a variety of plants, fungi and protists. Of particular importance is the finding that both emerging infectious diseases caused by human and plant fungal pathogens, the majority of which are multi-drug resistant, appear to be dependent upon AOX activity for survival. Since AOX is absent in mammalian cells, AOX is considered a viable therapeutic target for the design of specific fungicidal and anti-parasitic drugs.

In this work, we have mutated conserved residues within the hydrophobic channel (R96, D100, R118, L122, L212, E215 and T219), which crystallography has indicated leads to the active site. Our data shows that all mutations result in a drastic reduction in V_{max} and catalytic efficiency whilst some also affected the K_m for quinol and oxygen. The extent to which mutation effects inhibitor sensitivity was also investigated, with mutation of R118 and T219 leading to a complete loss of inhibitor potency. However, only a slight reduction in IC_{50} values was observed when R96 was mutated, implying that this residue is less important in inhibitor binding. *In silico* modelling has been used to provide insight into the reason for such changes, which we suggest is due to disruptions in the proton transfer network, resulting in a reduction in overall reaction kinetics. We discuss our results in terms of the structural features of the ubiquinol binding site and consider the implications of such findings on the nature of the catalytic cycle.

Significance

The alternative oxidase is a ubiquinol oxidoreductase enzyme that catalyses the oxidation of ubiquinol and the reduction of oxygen to water. It is widely distributed amongst the plant, fungal and parasitic kingdoms and plays a central role in metabolism through facilitating the turnover of the TCA cycle whilst reducing ROS production.

Keywords

Respiration, alternative oxidase, ubiquinone-binding, Trypanosoma brucei, electron transfer, drug-design

1. Introduction

The alternative oxidases (AOX) are important ubiquinol oxido-reductases which play a key role as terminal oxidases in the respiratory chains of plants, fungi and protists. AOXs are located on the substrate-side of the cytochrome bc_1 complex and catalyse the oxidation of ubiquinol and the four electron reduction of oxygen to water in a non-protonmotive fashion, with the excess energy being released as heat. Whilst the function of the protein is organism dependent, it is important to recognise that it is a major contributor to reducing cellular levels of reactive oxygen species through maintaining the ubiquinone pool in a relatively oxidised state, thereby preventing mitochondrial damage [1, 2]. Although thermogenic plants utilise the AOX for pollination purposes, [3, 4] all other plant cells and fungal pathogens tend to engage the AOX when respiratory activity is hindered either as a result of respiratory inhibition [5] or other stresses such as drought [6]. Of particular significance is the finding that a number of highly pathogenic protists, such as *Trypanosoma brucei* [7], *Cryptosporidium parvum* [8]*, Blastocystis hominis* [9] and the microsporidia all contain an AOX. Within these organisms, AOX plays a critical role during their respective life-cycles, with cases such as the *T. brucei* utilising the protein as its sole terminal oxidase whilst in its bloodstream form [10]. Since the protein is absent from mammals it has therefore become a novel therapeutic target for the treatment of diseases caused by such organisms [11].

Furthermore, the emergence of fungal infectious diseases is increasingly recognized as not only posing a world-wide threat to food security, but more recently pose a major threat to human and ecosystem health. The impacts of fungal diseases are clearly seen in cereal crops, such as wheat and rice in addition to maize, potatoes and soybean, and more recently emerging fungal infections are devastating world-wide cacao and banana plantations [12, 13]. In human diseases, in addition to the role of AOX in parasites, it also plays a key metabolic role in opportunistic human fungal pathogens such as *Candida albicans* [14]*, Candida auris* (candidiasis), and *Cryptococcus neoformans* (cryptococciosis)[15]. Immunocompromised individuals are not only particularly susceptible to infection by such opportunistic pathogens, but also to other emerging human pathogens possessing AOX.

Given the important cellular role of the AOX in the metabolism of such organisms, the need to control AOX activity is obvious. Ascofuranone is an extremely potent inhibitor of the trypanosomal AOX (TAO) [16] but as recently shown by May *et al*. this compound does not inhibit all alternative oxidases [17]. In an attempt to develop more species-specific inhibitors, we have investigated the quinone-binding site and its role within the catalytic cycle to determine suitable targets. Current predictions on the mechanism of oxygen reduction by the alternative oxidases [18] are based on the activity of other well defined di-iron proteins such as rubrerythrin [19], methane monooxygenase [20] and ribonucleotide reductase [21]. However, the lack of spectroscopic handle and the poor solubility of the purified AOX has made detection of intermediates, and therefore the determination of the complete catalytic cycle, difficult.

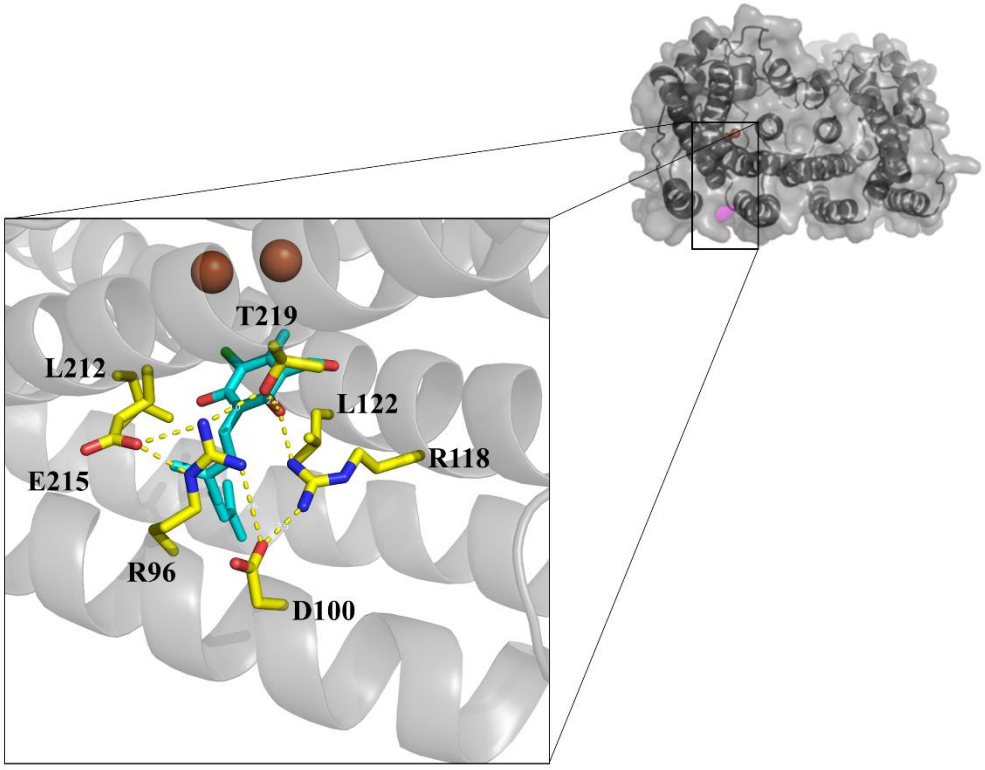

Figure 1: Position of the hydrophobic cavity within the AOX dimer. Magenta bulb in the surface diagram denotes the entrance. Hydrophobic cavity extending from the membrane between helices 1 and 4 towards the di-iron core. Insert depicts binding of the protein to the inhibitor colletochlorin B (cyan), with labelled residues being discussed within this manuscript. Yellow dotted lines depict the hydrogen bonding network between the residues and inhibitor. Coloured atoms are oxygen (Red), nitrogen (Blue) and chlorine (Green).

Examination of TAO crystal structures co-crystallised with inhibitors [22] have revealed a number of key polar residues for inhibitor binding that line the hydrophobic cavity leading from the membrane towards the di-iron core (Figure 1), namely R96, D100, R118, E215 and T219. Previous examination of sequence alignments [18] has shown that these amino acids are almost all fully conserved across all AOX's, with the exception of T219, which is a replaced by serine in select plant and fungal species [23]. These conserved residues can largely be divided up into two sub-groups; R96, R118, and T219, which all bind directly to the inhibitor via hydrogen bond formation, whereas D100 and E215 provide structural support to the former group of amino acids. The remaining highlighted residues, L122 and L212, form a hydrophobic bottleneck within the cavity, which we have previously proposed ensure the correct orientation of the substrate during its entry into the active site [24].

In this study we investigated the role of these amino acids (R96, D100, R118, L122, L212, E215 and T219) on substrate binding and oxygen reduction through the generation of residue specific mutations in recombinant TAO expressed in *Escherichia coli.* Each of these mutants were purified and assayed to assess the role of these residues on the overall reaction kinetics for both quinol and oxygen. We demonstrate that each of the mutations are critical for enzymatic activity, reducing the catalytic efficiency by approximately 95% in all cases. However, whilst the K_m for quinol was reduced for all the mutations that interact directly with the substrate, importantly no change in quinol K_m for the E215 variants were observed. Analysis of the K_m for oxygen revealed that mutational effects were minimal, confirming that reduction in the overall V_{max} is due to a structural impairment in quinol binding within the active site. *In silico* modelling suggested that the reason for such dramatic changes in kinetic properties is undoubtedly due to disruptions in the proton transfer network thereby resulting in a disruption of the catalytic cycle. Such studies have provided us with structural information on the binding of quinol within the active site of AOX which will be important in the subsequent design and development of potent anti-fungal and parasitic drugs targeted at the AOX.

2. Materials and methods

2.1. *Plasmid preparation and generation of mutants*

The design of rTAO was based on the *Trypanasoma brucei brucei* sequence (GenBank accession number: AB070617.1). Gene constructs were designed to introduce amino acid substitutions (residues as stated in the main text) and were synthesized with codon optimization for expression in *E. coli.* Constructs contained *Nde*I and *Bam*HI restriction endonuclease sites at 5' and 3' ends respectively, for insertion into the pET-15b expression vector (Genscript, Piscataway, NJ).

2.2. *Preparation of membrane samples*

The *E. coli* strain FN102(DE3) carrying the previously described pET-15b vectors containing cDNA for TAO, or subsequent mutant sequences, were pre-cultured at 37°C in L-broth [containing 100 μg ml^{-1} 5-aminolevulinic acid (ALA), 50 μg ml^{-1} ampicillin, 50 μg ml^{-1} kanamycin] for 4 hours. Cells were then collected by centrifugation at 7,000*g* for 15 min, with the subsequent pellet washed twice with L-broth to remove excess ALA. The pre-cultured cells were transferred into growth medium containing 40 g peptone, 20 g yeast extract, 20 g casamino acid, 41.6 g K_2HPO_4, 2.9 g trisodium-citrate, 10 g $(NH_4)_2SO_4$, 0.2 g $MgSO_4$, 0.1 g $FeCL_3$, 0.1 g $FeSO_4$, 0.2% (*w/v*) glucose, and 0.4 g carbenicillin. The culture was then initiated at OD_{600}= 0.01 at 30°C and expression of rTAO (and mutants) was induced by the addition of isopropyl β-D-1-thiogalactoside (IPTG) (25 μM) at OD_{600} = 0.6. Cells were harvested 12 hours following induction and were resuspended in 50 mM Tris-HCl (pH 7.5) containing protease inhibitor cocktail (Sigma) and broken by a French Pressure Cell at 10 kPa. Unbroken cells were removed by centrifugation at 10,500*g* for 15 min. *E. coli* membranes were collected by ultracentrifugation at 200,000*g* for 1 hour at 4°C. The membrane pellet was resuspended in 50 mM Tris-HCl (pH 7.5) to an approximate protein content of 12 mg ml^{-1}.

Protein content was estimated using the Bradford method [25], with the Bio-Rad protein assay dye using BSA as a standard.

2.3. *Protein Solubilisation and Purification Techniques*

Membranes were treated with solubilisation buffer (6 mg ml^{-1} protein in 50 mM Tris-HCl, 1.4% (*w/v*) n-octyl-β-D-glucopyranoside (OG), 200 mM $MgSO_4$, 20% (*v/v*) glycerol, pH 7.3) at 4°C for 1 h. The sample was then centrifuged at 200,000*g* for 1 h at 4°C, and the insoluble pellet was subsequently discarded.

Hybrid batch/column procedure described in manufacturer's instruction was used as stated below. 1 mL of resin (BD Bioscience, TALON Metal Affinity Resin) was equilibrated in a batch format by 10 mL of equilibration buffer (20 mM Tris-HCl, 1.4% (*w/v*) OG, 100 mM $MgSO_4$, 20% (*v/v*) glycerol pH 7.3). Two millilitre of solubilised protein was mixed with the resin for 20 min at 4°C. The resin was washed twice with 10 mL of wash buffer [20 mM Tris-HCl, 20 mM imidazole, 0.042% (*w/v*) n-dodecyl-β-D-maltopyranodise (DDM), 50 mM $MgSO_4$, 20% (*v/v*) glycerol, pH 7.3]. The rTAO was eluted with elution buffer [20 mM Tris-HCl, 250 mM imidazole, 0.042% (*w/v*) DDM, 50 mM $MgSO_4$, 60 mM NaCl, 20% (*v/v*) glycerol, pH 7.3].

2.4. *Measurement of Quinol and Oxygen Kinetics*

Kinetic analysis of purified rTAO was performed spectrophotometrically using Cary 400 UV spectrophotometer with the packaged software. All assays were performed using a quartz 1 cm cuvette with 1 ml 50mM Tris-HCl pH 7.4, 0.02% EDT-20, measuring the conversion of Q_1H_2 (ubiquinol-1) to Q_1 (ubiquinone-1) at 278 nm ($\mathcal{E}$ = 15, 000 M^{-1} cm^{-1}). Q_1 was reduced to Q_1H_2 prior to experimentation via sonication with zinc powder under an inert atmosphere for ~10 minutes, with the resultant zinc removed via centrifugation at 2000 x g.

Results were fit to Michaelis-Menten plot via a least squared method using GraphPad Prism version 7.0 for Windows, GraphPad Software, La Jolla California USA, www.graphpad.com.

Oxygen kinetics were obtained polarographically using a rank type oxygen electrode. *E. coli* membrane fractions were added to 2 ml 50 mM Tris-HCl pH 7.4 with 1 mM KCN and the reaction was initiated with the addition of 1.25 mM NADH. An oxygen consumption rate of ~1 nmol O_2 min^{-1} mg^{-1} was sufficient to allow enough data points to be collected for determination of O_2 K_m via an Eadie-Hofstee graph.

2.5. *Inhibitor dose response*

Inhibitors were tested in a 96-well plate format. *E. coli* membrane samples containing the appropriate AOX were diluted to ~ 60 µg ml^{-1} in 50 mM Tris-HCl (pH 7.5) containing 1 mM KCN. All inhibitors were dissolved in DMSO and added to the wells to a final concentration of 0.1% (*v/v*) DMSO. Respiration was initiated with an addition of 0.3 mM NADH and the reaction was tracked at 340 nm for 10 minutes using a Thermoscietific™ Multiskan Sky and packaged SkanIt 5.0 software. Dose response curves were plot using the least squared method in graphpad, with all data being shown as an average of 3 separate preparations ± SEM.

2.6. *Computational Methods*

The TAO protein structure (PDB:3W54) was loaded into MOE software (Molecular Operating Environment, version 2016.08, Chemical Computing Group Inc., Montreal, Canada) for some preparatory steps to correct any structural issues. Hence, the hydrogen bond network was optimised using the Protonate 3D algorithm and AMBER99 forcefield was used in assigning correct electronic charges. Mutations were then subsequently generated, followed by sequential local energy minimization and a full system minimization using the AMBER99 forcefield.

The 3D structure for Q_2H_2 (ubiquinol-2) was built within MOE and energy minimized using the Amber10: EHT forcefield. A second minimization was applied using the MOPAC semi-empirical energy functions (PM3 Hamiltonian).

Q_2H_2 was docked into the binding site of the AOX using the Triangle Matcher placement method with London dG scoring. Subsequently, poses resulting from the placement stage were further refined using the Induced Fit method, which allows protein flexibility upon ligand binding, improving the prediction accuracy for the interaction. Poses were rescored using the GBVI/WSA dG scoring function and the top five best scoring poses were retained and evaluated manually.

2.7. *Materials*

All reagents were purchased from Sigma-Aldrich unless otherwise stated. Of the inhibitors tested, samples of ascochlorin and ascofuranone were kindly provided by Professor Saimoto (Tottori University) Colletochlorin B and D was synthesised in house using previously published methods [26].

2.8. *Statistical analysis*

All statistical analysis was performed in GraphPad prism 7.0. Where quoted, all averages displayed are a mean average of 3 replicates ± SEM. Where relevant, p values were determined using a 1-way ANOVA test, with comparisons being made to the wild type.

3. Results

3.1 *Recombinant protein expression*

Recombinant wild type and mutant rTAO protein was obtained from heme-deficient *E. coli* membrane fraction and purified via cobalt affinity chromatography as described within in Materials and Methods, which we have previously shown to be effective at generating stable purified rTAO [27]. Purity of the protein was assessed via SDS-gel and western blot analysis, with each preparation giving a single band at ~32 kDa (data not shown).

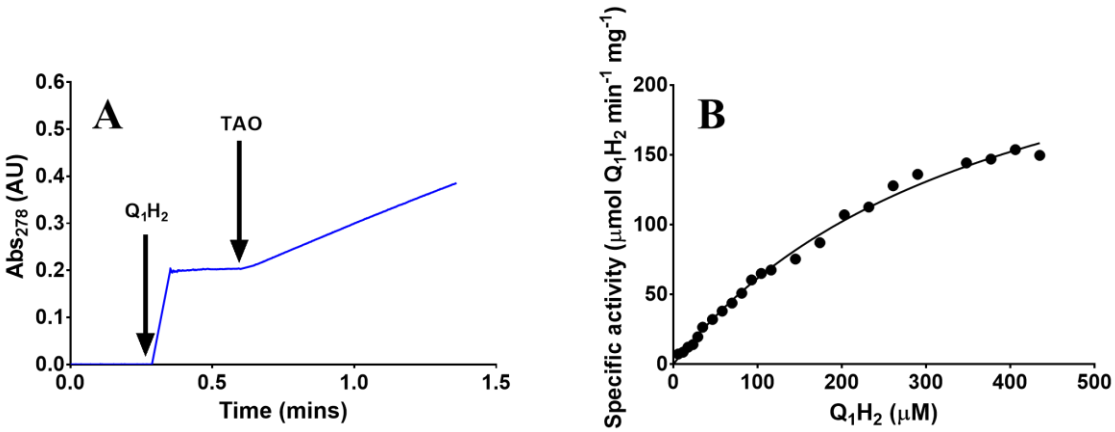

Figure 2: A) Example quinol oxidation trace for purified rTAO. ↓ denotes addition of Q_1H_2 and purified rTAO protein to allow for determination of auto-oxidation rate and protein Q_1H_2 consumption rate respectively. B) Michaelis-Menten graph for purified rTAO. Analysis was performed in 1 ml of Tris-HCl pH 7.4 with Q_1H_2 concentrations varied between 10-500 μM. Values were determined by fitting the data to a Michaelis-Menten curve via the least squared method using the GraphPad Prism 7.0 software.

TAO	V_{max} (µmol Q_1H_2 min^{-1} mg^{-1})	V_{max} (% of wild-type)	Catalytic efficiency (s^{-1} M^{-1})
Wild-type	270 ± 28	100	$9.18 \times 10^5 \pm 0.3$
R96A	4.32 ± 3.1	1.6 ± 1.1	$1.16 \times 10^5 \pm 0.3$
R96K	5.39 ± 3.2	2.0 ± 1.2	$1.17 \times 10^5 \pm 0.5$
D100A	2.48 ± 1.1	0.9 ± 0.4	$1.04 \times 10^5 \pm 0.3$
D100E	4.16 ± 2.2	1.5 ± 0.8	$1.62 \times 10^5 \pm 0.4$
R118A	5.85 ± 0.9	2.1 ± 0.3	$4.08 \times 10^4 \pm 1$
R118K	9.59 ± 3.5	3.6 ± 1.3	$4.66 \times 10^4 \pm 1$
T219A	3.57 ± 1.4	1.3 ± 1.0	$2.52 \times 10^4 \pm 0.7$
T219S	1.41 ± 0.3	0.5 ± 0.1	$1.03 \times 10^4 \pm 0.1$
L122A	2.47 ± 1.7	0.9 ± 0.6	$2.67 \times 10^4 \pm 1$
L212A	4.20 ± 0.2	1.5 ± 0.1	$2.94 \times 10^4 \pm 0.7$
E215A	8.08 ± 1.9	2.9 ± 0.7	$2.70 \times 10^4 \pm 0.02$
E215D	0.68 ± 0.6	0.2 ± 0.2	$1.74 \times 10^3 \pm 0.9$
E215N	0.49 ± 0.04	0.2 ± 0.0	$1.62 \times 10^3 \pm 0.02$

Table 1: V_{max} and catalytic efficiency values determined for purified wild type rTAO and mutants, using the method outlined in figure 2. All data presented as an average of 3 measurements ± SEM.

Kinetic analysis of the purified protein was performed by measuring the rate of Q_1H_2 oxidation at 278 nm, with the determined rates subsequently plotted in a Michaelis-Menten graph as depicted in Figure 2. The selected residues were initially mutated to alanine to assess the importance of each side-chain to the overall reaction kinetics, and as can be seen in Table 1, each alanine substitution resulted in over 95% reduction in V_{max} when compared to wild-type. Further secondary mutations were generated based on retention of function of the initial side-chain, with selection being made for keeping the same charge (R96K, R118K and T219S) or complete retention of the carboxylate functionality but with a modification in side-chain length (D100E and E215D). It is apparent from Table 1 that some secondary mutations appeared to partially restore catalytic activity. For instance R96K, D100E and R118K all show a slight increase in catalytic activity over their alanine counterparts, whereas T219S and E215D/N show a further decrease in their respective V_{max} values, suggesting they are more detrimental to overall kinetic activity than simply removing the amino acid side chain.

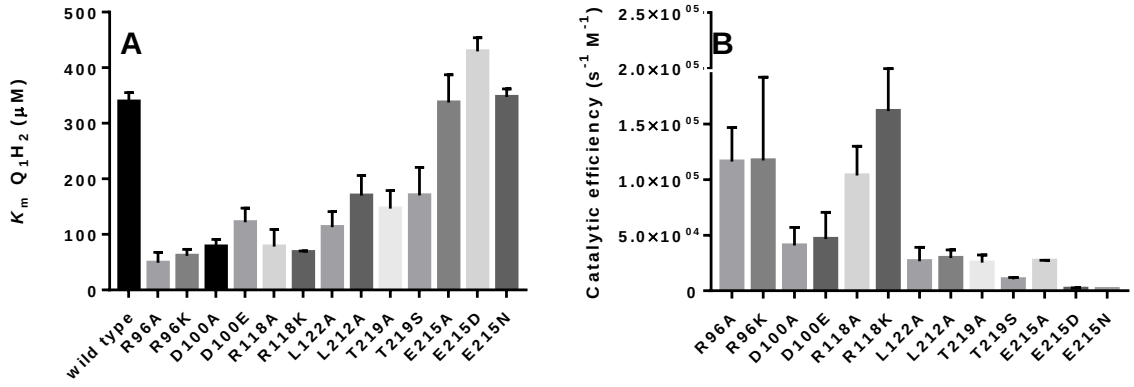

Figure 3: A) Effects of mutation upon the K_m for quinol. B) Catalytic efficiency of mutants. rTAO wild-type omitted for clarity, giving a value of $9.2 \times 10^5 \pm 0.3\ s^{-1}$.

As is apparent from Figure 3, there is a significant change (p=0.0001) in the K_m for Q_1H_2 for all mutations, with the exception of the E215 mutations. Of the three residues that bind directly to quinol, T219A/S shows a significantly less pronounced reduction in Q_1H_2 K_m values when compared to R96 and R118 mutations. Whilst the crystal structures of TAO indicate that D100 does not interact directly with the inhibitor (PDB:3w54 [22]), and therefore the substrate, the reduction in K_m value would suggest that its role in structurally supporting both R96 and R118 is important for quinol binding, as the K_m value is reduced to a similar extent. As observed with V_{max}, secondary mutations do not significantly alter the K_m for quinol when compared to their alanine counterparts.

Given the large reduction in V_{max} and K_m for each mutation, calculation of the catalytic efficiency (defined as K_{cat}/K_m) allows for clearer comparison of the mutation effect upon the overall activity as it takes into account changes to both the V_{max} and the K_M values. Using this metric it is apparent that the mutation of both R96 and R118 are considerably less detrimental then the other mutants, reducing catalytic efficiency to $1.2 \times 10^5 \pm 0.3\ s^{-1}$ (R96A) and $1.1 \times 10^5 \pm 0.2\ s^{-1}$ (R118A) respectively from $9.2 \times 10^5 \pm 0.3\ s^{-1}$ for the wild type. Given the positioning of the quinol OH between R96, R118 and T219, we can infer that the interaction with T219 is the most important of the three when it comes to catalytic activity, suggesting that both R96 and R118 fulfil a similar role in stabilising the orientation of the quinol OH, with both residues being necessary to position the OH towards T219.

What was surprising, however, was the result that E215D/N mutations have the largest effect on the catalytic efficiency, suggesting that whilst they are not directly involved in the binding of the substrate, they must perform a critical role in the catalytic cycle. It is also worth noting that the catalytic efficiency of the secondary mutations were considerably lower than their alanine counterpart, with the E215D and E215N mutants possessing values of $1.7 \times 10^4 \pm 0.9\ s^{-1}$ and $1.6 \times 10^4 \pm 0.1\ s^{-1}\ M^{-1}$ respectively, an order of magnitude lower than their E215A counterpart which has a catalytic efficiency of $2.6 \times 10^5 \pm 0.4\ s^{-1}\ M^{-1}$.

3.2 *Oxygen Kinetics*

The K_m for oxygen was determined in the same manner as previously used for recombinant *Saromatum guttatam* AOX and mutants [24]. Recombinant rTAO grown in the heme-deficient *E. coli* strain is responsible for ~98% of total oxygen consumption with the remaining 2% being attributed to cytochromes b_d/b_o activity. In the presence of an excess of NADH within these assays, any loss of respiratory activity following the establishment of steady state kinetics can be attributed solely to the reduction in the concentration of oxygen within the chamber, with the relationship between oxygen concentration and respiratory rate obeying standard Michaelis-Menten kinetics. This in turn allows for the determination of oxygen K_m values via Eadie-Hofstee graphs.

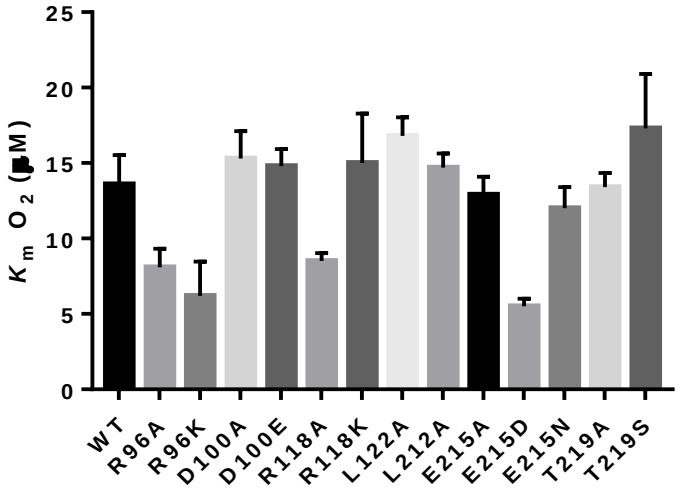

Figure 4: - Oxygen K_m values determined using method described figure 4 Data is an average of 3 replicates +/- SEM. Numerical values can be found in the Appendix Table 1.

The data in figure 4 demonstrates that a majority of these mutations have little effect on the K_m for oxygen, with only R96A/K (p=0.0081 and 0.0003), R118A (p=0.0161) E215D (p=0.0001) altering the K_m with any statistical significance. Both R96A/K mutations have a lower K_m value, whereas only R118A and E215D show any effect on the oxygen K_m within their respective amino acid substitutions, implying that these two amino acid substitutions are more deleterious to oxygen binding than simply removing the amino acid side chain. It is Interesting to note that the D100 mutations did not alter the oxygen K_m, which is in contrast to previous results obtained with the analogous mutation in the *Sauromatum guttatum* rAOX [24].

3.3 *Mutant Inhibitor dose response*

In order to further assess the impact of mutations within the quinol binding site, dose response curves were determined using a range of AOX inhibitors. Of those tested, octyl-gallate (OG) and Salicylic hydroxamic acid (SHAM) are classic inhibitors of AOX with relatively low inhibitory efficacy, with the remaining 4 compounds being quinol mimetic inhibitors which are believed to be transition state analogues for quinol [28].

Mutation	AC	AF	CB	CD	OG	SHAM
Wild-type	7.4 ± 3	7 ± 5	7.5 ± 1	33 ± 5	230 ± 6	6.1 µM
R96A	167 ± 55	58 ± 24	470 ± 225	1.54 ± 0.3 µM	46 ± 25 µM	22 µM
R96K	316 ± 96	129 ± 30	66 ± 25	51 ± 5	2.3 ± 1.5 µM	4.4 µM
D100A	203 ± 14	51 ± 5	137± 18	81 ± 16	308 ± 45	4.4 µM
D100E	221 ± 19	89 ± 14	139± 11	90 ± 15	5.2 ± 1.1 µM	3.7 µM
R118A	NI	NI	NI	NI	NI	NI
R118K	NI	NI	NI	NI	NI	NI
T219A	NI	NI	NI	NI	NI	NI
T219S	NI	NI	NI	NI	NI	NI
L122A	NI	NI	NI	NI	NI	NI
L212A	215 ± 22	38 ± 4	36 ± 8	61 ± 15	862 ± 120	4.7 µM
E215A	NI	NI	NI	NI	NI	NI
E215D	NI	NI	NI	NI	NI	NI
E215N	NI	NI	NI	NI	NI	NI

Table 2: IC_{50} values for AOX inhibitors against each membrane bound mutation. Compounds tested are as follows: Ascochlorin (AC), Ascofuranone (AF), Colletochlorin B (CB), Colletochlorin D (CD), Octyl-gallate (OG) and Salicylic hydroxamic acid (SHAM). All values denoted are in nM and displayed as an average of 3 repeats ± SEM. NI indicates an IC_{50} >50µM.

As is apparent from Table 2, there is a distinct split in effects on inhibitor efficacy. Mutation of R118 and T219, two of the residues that interact directly with colletochlorin B in the crystal structure [22], lead to a complete loss of inhibition. However, there is

only a slight reduction in IC_{50} values when R96 is mutated, which implies that this residue is less important to the binding of the inhibitor than we previously thought. With respect to the leucine residues, mutation of L122 is clearly more detrimental when it comes to inhibition, although whether this is due to reduction in binding efficacy of the compound or alteration to the pocket shape remains to be determined. What was surprising, however, was the complete lack of inhibition with respect to the E215 mutations, given that they are not directly involved in inhibitor binding.

3.4 *Substrate docking*

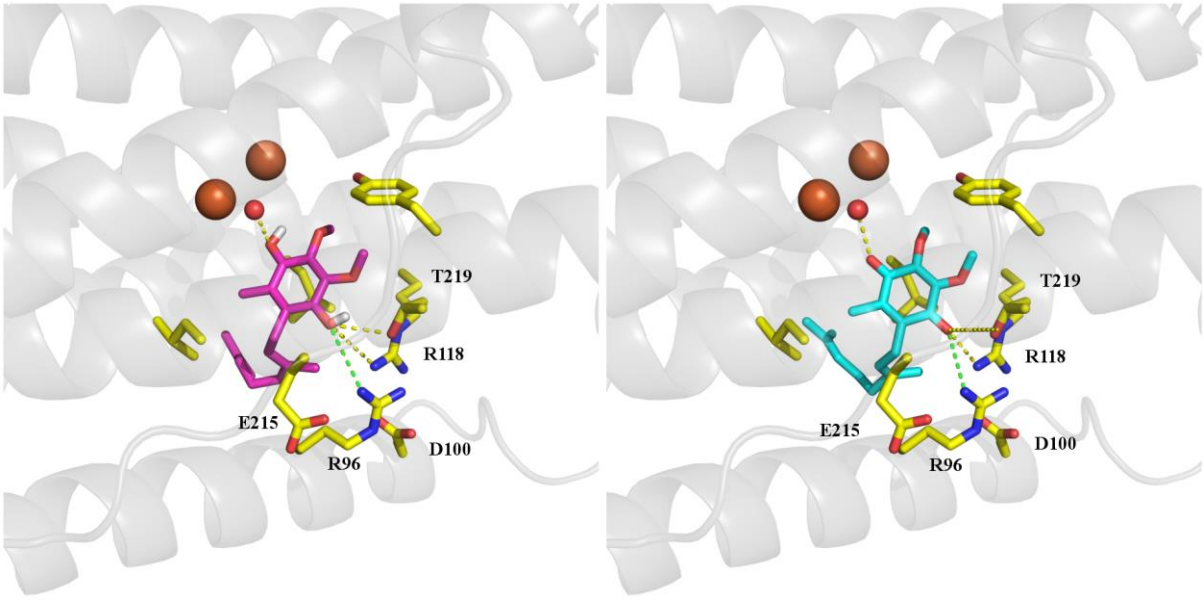

Figure 5: Docking studies for Quinol (magenta) and Quinone (cyan) within the TAO crystal structure (PDB:3W54). Yellow dotted lines denote potential hydrogen bond formation (distance less than 3.5 Å) between quinone species and residues within the cavity, and the green dotted line denotes the increased 4.5 Å from R96 to the substrate.

In order to ensure that the residues responsible for inhibitor binding are also all involved in substrate binding, docking of quinol was performed on the crystal structures. Whilst the natural substrate for TAO is $Q_{10}H_2$, Q_2H_2 was used for docking purposes as the longer isoprene tail extended out of the hydrophobic cavity (which,

under physiological conditions would pass into the phospholipid bilayer within mitochondria) and hence resulted in erroneous binding along the outside of the protein, artificially improved the binding score. Figure 5 shows the lowest ΔG_{bind} (z=-8.7 kcal mol^{-1}) that was obtained with Q_2H_2, with the formation of hydrogen bonds between OH-2 and the iron ligating OH/H_2O (3.1 Å) and OH-5 bonding to T219 (2.6 Å) and R118 (3.0 Å). The distance to R96 has increased to from 3.5 Å for the bound Colletochlorin B within the crystal structure to 4.5 Å for the docked quinol, indicating that while it is an important hydrogen bond donor for the inhibitors, it is not likely to be involved directly with substrate binding.

To ensure that the changes in apparent substrate K_m were not due to changes in product binding, quinone was also docked, and as can be seen in Figure 5 both compounds are able to bind effectively into the active site in its current configuration, with quinone demonstrating a slightly higher ΔG_{bind} than quinol (z= -9.2 kcal mol^{-1}). Whilst this is the case for the protein in its current protonation state, it should be noted that when quinone is generated as a product of the oxidation reaction, the protonation state of the binding site will be altered and the quinone will be more able to leave the active site.

Mutation	Quinol binding ΔG_{bind} (kcal mol^{-1})	Quinone binding ΔG_{bind} (kcal mol^{-1})	Ratio Quinol/Quinone
Wild-type	-8.7 ± 0.1	-9.2 ± 0.2	0.95
R96A	-8.6 ± 0.3	-8.9 ± 0.2	0.96
R96K	-8.8 ± 0.1	-9.0 ± 0.2	0.98
D100A	-8.8 ± 0.2	-9.1 ± 0.1	0.97
D100E	-8.7 ± 0.1	-9.1 ± 0.2	0.95
R118A	-8.3 ± 0.2	-8.4 ± 0.3	0.98
R118K	-8.5 ± 0.2	-8.8 ± 0.1	0.96
T219A	-6.7 ± 0.1	-6.8 ± 0.1	0.98
T219S	-6.6 ± 0.2	-7.3 ± 0.4	0.91
L122A	-8.0 ± 0.1	-8.2 ± 0.2	0.96
L212A	-7.4 ± 0.1	-7.1 ± 0.1	1.05
E215A	-7.6 ± 0.6	-7.5 ± 0.2	1.00
E215D	-6.6 ± 0.1	-6.8 ± 0.1	0.97
E215N	-6.7 ± 0.1	-7.0 ± 0.2	0.96

Table 3: Docking scores determined for quinol and quinone against energy minimised point mutations generated within the MOE software. Each score given is an average of the top 3 poses ± standard deviation.

The mutants were then generated from the crystal structure and energy minimised, with both Q_2 and Q_2H_2 subsequently docked to investigate the effects on substrate binding. All docked compounds were checked manually and found to adhere to similar binding positions as the inhibitor determined in the wild-type crystal structure. As can be seen in Table 3, most of the mutations generated did not affect the ability of the substrate to bind to the protein, with only the mutations of T219, L212 and E215 being significantly different to that of the wild type.

The ratio of Q_2 to Q_2H_2 docking scores were also determined and found not to vary wildly from the 0.96 determined for the wild-type. Such data would indicate that whilst there are large changes in the apparent K_m determined experimentally, this is unlikely to be a result of changes in the level of product inhibition artificially altering the K_m.

4 Discussion

The ubiquitous nature of the AOX throughout fungal pathogens and its central role within cellular homeostasis within these organisms has highlighted a need to develop specific AOX inhibitors for the use alongside traditional fungicidal treatment. Whilst the ascofuranone analogues investigated within this manuscript are extremely potent, only ascofuranone is specific for the AOX, with the other compounds also inhibiting the cytochrome bc_1 complex [29]. Albeit that such results indicate ascofuranone as the clear lead compound, the lengthy and costly synthesis precludes chemical synthesis [30], however generation of these compounds using the biosynthetic pathway has become a more viable option [31].

We have started to probe the mechanism of action of the AOX, with the primary focus to understand the catalytic cycle in order to allow for the development of 'suicide inhibitors' for the AOX, which would reduce the undesired interactions with the cytochrome bc_1 complex if they are tuned to specific intermediates in the AOX's catalytic cycle. Elucidation of the TAO crystal structure has allowed for a more detailed picture of the active site, and we have suggested a number of potential mechanisms based on this information [28, 32]. A previous study using FTIR [33] has confirmed that the fully oxidised di-iron core reacts with 2 molecules of quinol in a sequential manner, and we are working under the assumption that the crystal structure exists as the oxidised form of the protein, due to the crystal being obtained under non-reducing conditions. Within this study, we have utilised mutagenesis to investigate the reaction sequence upon binding of the first quinol within the hydrophobic cavity in order to narrow down the roles for each of the residues suggested to be involved in inhibitor binding from crystallography.

While the size and shape of the hydrophobic cavity varies between species [17], the majority of the polar residues which line the cavity are conserved throughout the AOX family. Given the importance of polar residues for binding and proton transfer, and the lack of other potentially reactive residues within the cavity, we are working under the assumption that there is a universal catalytic mechanism throughout the AOXs. What is clear from the outset of these results is that each of the residues selected for mutation are extremely important to overall activity, with each amino acid substitution

causing at least a 95% reduction in the V_{max} (Table 1). However, with the exception of R96/118 and E215D, there are no significant changes in the oxygen reaction kinetics (Figure 4), which would suggest that the overall structure of the protein is intact, and that di-iron core is in the correct conformation to react with oxygen. This would also confirm that the reaction of the fully reduced protein with oxygen and quinol are completely separate events which do not require either of the molecules of quinol to facilitate the binding of oxygen as there are limited changes to the oxygen kinetics whilst the K_m for quinol is altered in almost all cases. Moreover, when the models for quinol docking into the mutants were generated and minimised, negligible changes to the overall structure outside of the amino acid side chain were detected.

With respect to the changes in O_2 K_m for R96/118, given the distance of these residues from the oxygen reactive iron centre, and the lack of perturbation observed around the primary ligation sphere in the protein modelling, it is unlikely this has been caused by changes in reactivity between oxygen and the di-iron core. We hypothesise this apparent change in K_m is caused by an increase in solvent accessibility into the hydrophobic cavity via an opening that is visible in the protein surface during the molecular modelling, allowing oxygen to diffuse more freely into the di-iron core, increasing localised O_2 concentration and artificially improving the apparent O_2 K_m. With E215D being the only mutation of E215 to affect oxygen kinetics, it is likely that this is due to distortion of the position of R96 and opening a similar pore in the proteins surface. It would therefore follow that any changes in the overall reaction kinetics are predominantly due to changes in reactivity between the protein and quinol.

In isolation, the lowered K_m values for quinol observed in the mutants would imply a higher affinity for quinol, and therefore an increase in overall activity would be anticipated. This is clearly not the case, as the V_{max} has dropped considerably in all cases and the docking scores (Table 3) show minimal changes. Given that the reduction in V_{max} may have artificially reduced the quinol K_m value, the catalytic efficiency was calculated since it provides a less biased metric on the effects of each mutation. Figure 3 clearly demonstrates that all mutations result in a reduction in the overall reaction kinetics, since all possess a catalytic efficiency significantly lower than the wild type.

What is clear from the inhibition studies (Table 2) is that there is a significant split in the importance of residues with respect to inhibitor binding. R96, D100 and L212 reduce inhibitory efficacy by 5-40 fold, whereas all other mutations led to a complete loss of efficacy. However, the docking studies demonstrated that while these residues are important for inhibitor binding, only mutations of T219, L212 and E215 significantly altered the binding ability of the substrate. Given that it has recently been suggested that the ascofuranone family of compounds behave as transition state analogues [28], which in the case of AOX turnover would likely constitute a semi-quinone radical, we propose the following roles for each residue based on the data collected within this study:

Since L212A reduced the binding efficacy of the substrate but the reduction in inhibition was relatively small, we suggest that the reduction in V_{max} can be attributed to a reduced substrate binding affinity. However, mutations of R96 and D100 had no effect on the docking score and only a slight reduction in inhibitor potency, suggesting that the reduction in catalytic activity is not due to binding affinity but more likely to be mechanistic or structural in nature.

The remaining residues, R118, L122 and T219, resulted in a complete eradication of inhibitor potency, implying they are involved with keeping the semiquinone radical bound during the transition state. This is inline with recent protein ligand interaction fingerprint (PLIF) experiments, which suggested that these are the most important residues when it comes to inhibitor interactions, and are therefore the most likely candidates to be stabilising the semi-quinone intermediate [34]. However, only the T219 mutants altered the docking score as well, indicating it is the only residue that fully interacts with both the substrate and its transition state.

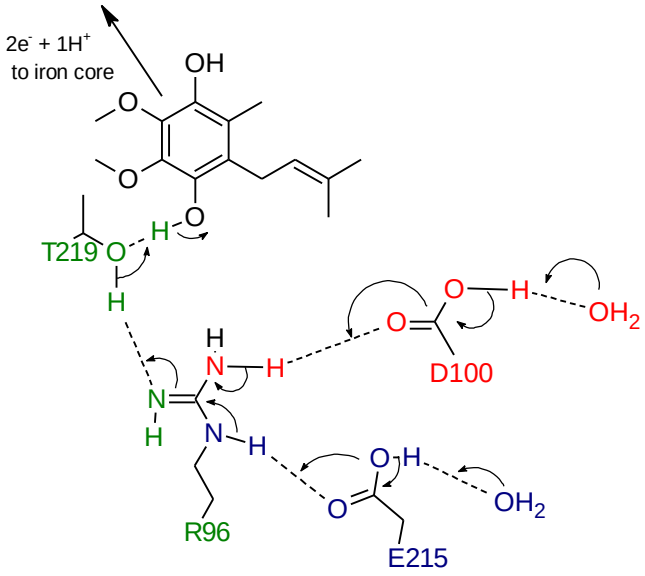

Figure 6: The two proposed routes for the proton relay pathway, with water molecules indicating the aqueous environment. Green Residues are common in both pathways, with red denotes the D100 pathway predicted in [32] and blue is the pathway predicted by Shiba et al. [28]. R118 has been omitted for clarity.

T219, R96, R118, E215 have also been proposed to be involved in an additional role in quinol oxidation, namely in the provision of a proton relay pathway to solvent (Figure 6) [28, 32]. We would suggest that D100 also plays a role within this network given the lack of any effects on either the docking or inhibition studies. There is, however, a potential catalytic redundancy between R96 and R118, as both offer routes of egress for a proton away from the active site. R96 is bound to both E215 and D100, which are both solvent facing residues, whereas R118 is only bound to D100. Energy minimisation of the protein revealed that whilst the crystal structure shows D100 is bound in a bidentate form, it is fully capable (and arguably energetically favourable) to bridge the R96 – R118 distance in a monodentate fashion, as depicted in Figure 7. Whilst purely speculative at this point, this relative freedom of movement would allow for easy solvent access.

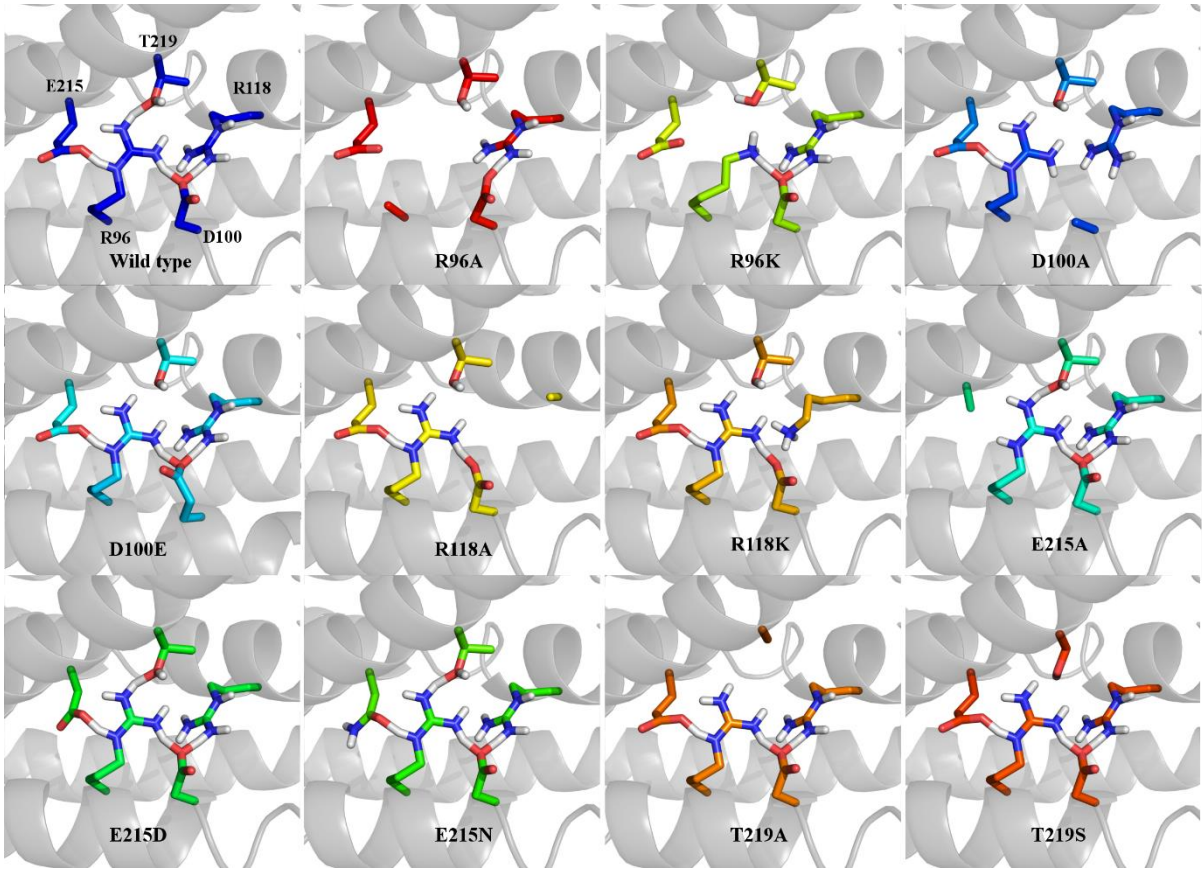

Figure 7: Molecular modelling of the hydrogen bonding network for Wild-type TAO and mutants. Coloured atoms are oxygen (red), nitrogen (blue) and hydrogen (white), where heteroatoms joined by a white line denote species which are close enough for hydrogen bond formation between the pair. L122/212 not included as they showed no effect on the proton transfer network.

If this proposal is correct, and the breakdown of the proton transfer network is responsible for the reduction in overall reaction kinetics, it would explain why the mutation of E215 has such a large effect on the overall activity whilst not effecting the K_m for quinol. Figure 7 shows putative proton transfer networks, and as can clearly be seen, all mutations lead to a breakdown of the network, with the exception of the E215 mutations. This lack of network breakdown, with particular focus of the T219-R96 hydrogen bond, would leave the binding to quinol unaffected. The change in residue would still lead to a change in electronic effect throughout the network, potentially reducing the networks ability to shuttle protons from the active site. However, given the abundant nature of protons within an aqueous solution, this would be extremely difficult to establish experimentally. It should also be noted that the terminus of the proton transfer network for both E215D and E215N point back into the protein instead of out to solvent, providing a further barrier for proton egress from the system.

In conclusion, we have mutated residues within the hydrophobic cavity of the trypanosomal AOX which crystallographic studies identified as being key for substrate and inhibitor binding. Amino-acid sequence analysis of all published AOX proteins revealed that these residues were totally conserved suggesting they are essential for substrate-binding. Measurement of catalytic activity confirmed the essentiality of these residues since every mutation resulted in a loss of >95% activity in comparison to the wild-type. Furthermore, such mutations also result in a substantial decrease in inhibitor efficacy. Whilst it would be extremely difficult to predict potential mutations *in vivo*, which could generate resistance to these compounds, this study has demonstrated that inhibitors that target the polar residues within the hydrophobic cavity are highly unlikely to lead to the generation of AOX proteins which are resistant to the inhibitor whilst retaining functionality.

Funding

ALM gratefully acknowledges the support by BBSRC (BB/L022915/1 and BB/NO10051/1)

References

1. Maxwell, D.P., Y. Wang, and L. McIntosh, *The alternative oxidase lowers mitochondrial reactive oxygen production in plant cells.* Proceedings of the National Academy of Sciences of the United States of America, 1999. **96**(14): p. 8271-6.
2. Vanlerberghe, G.C., *Alternative oxidase: a mitochondrial respiratory pathway to maintain metabolic and signaling homeostasis during abiotic and biotic stress in plants.* Int J Mol Sci, 2013. **14**(4): p. 6805-47.
3. Seymour, R.S., M. Gibernau, and K. Ito, *Thermogenesis and respiration of inflorescences of the dead horse arum Helicodiceros muscivorus, a pseudo-thermoregulatory aroid associated with fly pollination.* Functional Ecology, 2003. **17**(6): p. 886-894.
4. Meeuse, B.J.D., *Thermogenic respiration in aroids.* Annu Rev Plant physio, 1975. **26**: p. 117-126.
5. Vanlerberghe, G.C., C.A. Robson, and J.Y. Yip, *Induction of mitochondrial alternative oxidase in response to a cell signal pathway down-regulating the cytochrome pathway prevents programmed cell death.* Plant Physiol, 2002. **129**(4): p. 1829-42.
6. Vanlerberghe, G.C., G.D. Martyn, and K. Dahal, *Alternative oxidase: a respiratory electron transport chain pathway essential for maintaining photosynthetic performance during drought stress.* Physiol Plant, 2016. **157**(3): p. 322-37.
7. Grant, P.T., J.R. Sargent, and J.F. Ryley, *Respiratory systems in the Trypanosomidae.* Biochem J, 1961. **81**: p. 200-6.
8. Williams, B.A., et al., *A broad distribution of the alternative oxidase in microsporidian parasites.* PLoS Pathog, 2010. **6**(2): p. e1000761.
9. Tsaousis, A.D., et al., *The Human Gut Colonizer Blastocystis Respires Using Complex II and Alternative Oxidase to Buffer Transient Oxygen Fluctuations in the Gut.* Front Cell Infect Microbiol, 2018. **8**: p. 371.
10. Bienen, E.J., et al., *Non-cytochrome mediated mitochondrial ATP production in bloodstream form Trypanosoma brucei brucei.* Eur J Biochem, 1993. **216**(1): p. 75-80.
11. Nihei, C., Y. Fukai, and K. Kita, *Trypanosome alternative oxidase as a target of chemotherapy.* Biochimica Et Biophysica Acta-Molecular Basis of Disease, 2002. **1587**(2-3): p. 234-239.
12. Hebbar, P.K., *Cacao diseases: a global perspective from an industry point of view.* Phytopathology, 2007. **97**(12): p. 1658-63.
13. Meinhardt, L.W., et al., *Moniliophthora perniciosa, the causal agent of witches' broom disease of cacao: what's new from this old foe?* Mol Plant Pathol, 2008. **9**(5): p. 577-88.
14. Ruy, F., A.E. Vercesi, and A.J. Kowaltowski, *Inhibition of specific electron transport pathways leads to oxidative stress and decreased Candida albicans proliferation.* J Bioenerg Biomembr, 2006. **38**(2): p. 129-35.
15. Trevijano-Contador, N., et al., *Capsule Enlargement in Cryptococcus neoformans Is Dependent on Mitochondrial Activity.* Front Microbiol, 2017. **8**: p. 1423.
16. Minagawa, N., et al., *An antibiotic, ascofuranone, specifically inhibits respiration and in vitro growth of long slender bloodstream forms of Trypanosoma brucei brucei.* Mol Biochem Parasitol, 1996. **81**(2): p. 127-36.
17. May, B., L. Young, and A.L. Moore, *Structural insights into the alternative oxidases: are all oxidases made equal?* Biochem Soc Trans, 2017. **45**(3): p. 731-740.
18. Moore, A.L., et al., *Unraveling the heater: new insights into the structure of the alternative oxidase.* Annu Rev Plant Biol, 2013. **64**: p. 637-63.
19. Dillard, B.D., et al., *A cryo-crystallographic time course for peroxide reduction by rubrerythrin from Pyrococcus furiosus.* J Biol Inorg Chem, 2011. **16**(6): p. 949-59.

20. Tinberg, C.E. and S.J. Lippard, *Revisiting the mechanism of dioxygen activation in soluble methane monooxygenase from M. capsulatus (Bath): evidence for a multi-step, proton-dependent reaction pathway.* Biochemistry, 2009. **48**(51): p. 12145-58.
21. Tomter, A.B., et al., *Ribonucleotide reductase class I with different radical generating clusters.* Coordination Chemistry Reviews, 2013. **257**(1): p. 3-26.
22. Shiba, T., et al., *Structure of the trypanosome cyanide-insensitive alternative oxidase.* Proc Natl Acad Sci U S A, 2013. **110**(12): p. 4580-5.
23. McDonald, A.E., *Alternative oxidase: what information can protein sequence comparisons give us?* Physiol Plant, 2009. **137**(4): p. 328-41.
24. Young, L., et al., *Probing the ubiquinol-binding site of recombinant Sauromatum guttatum alternative oxidase expressed in E. coli membranes through site-directed mutagenesis.* Biochim Biophys Acta, 2014. **1837**(7): p. 1219-25.
25. Bradford, M.M., *A rapid and sensitive method for the quantitation of microgram quantities of protein utilizing the principle of protein-dye binding.* Anal Biochem, 1976. **72**: p. 248-54.
26. Elliott, C., et al., *Purification and characterisation of recombinant DNA encoding the alternative oxidase from Sauromatum guttatum.* Mitochondrion, 2014. **19 Pt B**: p. 261-8.
27. Kido, Y., et al., *Purification and kinetic characterization of recombinant alternative oxidase from Trypanosoma brucei brucei.* Biochim Biophys Acta, 2010. **1797**(4): p. 443-50.
28. Shiba, T., et al., *Insights into the ubiquinol/dioxygen binding and proton relay pathways of the alternative oxidase.* Biochim Biophys Acta Bioenerg, 2019. **1860**(5): p. 375-382.
29. Berry, E.A., et al., *Ascochlorin is a novel, specific inhibitor of the mitochondrial cytochrome bc1 complex.* Biochim Biophys Acta, 2010. **1797**(3): p. 360-70.
30. Mori, K. and T. Fujioka, *Synthetic Microbial Chemistry .4. Synthesis of (+/-)-Ascochlorin, (+/-)-Ascofuranone and Ll-Z1272-Alpha.* Tetrahedron, 1984. **40**(14): p. 2711-2720.
31. Araki, Y., et al., *Complete biosynthetic pathways of ascofuranone and ascochlorin in Acremonium egyptiacum.* Proc Natl Acad Sci U S A, 2019. **116**(17): p. 8269-8274.
32. Young, L., et al., *Structure and Mechanism of Action of the Alternative Quinol Oxidases.* Cytochrome Complexes: Evolution, Structures, Energy Transduction, and Signaling, 2016. **41**: p. 375-394.
33. Marechal, A., et al., *Three redox states of Trypanosoma brucei alternative oxidase identified by infrared spectroscopy and electrochemistry.* J Biol Chem, 2009. **284**(46): p. 31827-33.
34. Alicia Rosell-Hidalgo, L.Y., Anthony L. Moore, Taravat Ghafourian, *QSAR and molecular docking for the search of AOX inhibitors: a rational drug discovery approach.* Journal of computer-Aided Molecular Design (Submitted), 2020.

APPENDIX

Mutation	K_m Q_1H_2 (µM)	Catalytic efficiency (s^{-1} M^{-1})	K_m Oxygen (µM)
Wild-type	339.0 ± 16	9.18 x 10^5 ± 0.3	13.6 ± 1
R96A	48.8 ± 19	1.16 x 10^5 ± 0.3	8.1 ± 1
R96K	61.3 ± 12	1.17 x 10^5 ± 0.5	6.2 ± 2
D100A	78.2 ± 13	1.04 x 10^5 ± 0.3	15.3 ± 1
D100E	121.7 ± 26	1.62 x 10^5 ± 0.4	14.8 ± 1
R118A	78.3 ± 30	4.08 x 10^4 ± 1	8.5 ± 0.5
R118K	68.0 ± 2	4.66 x 10^4 ± 1	15 ± 2
T219A	113.3 ± 27	2.52 x 10^4 ± 0.7	13.4 ± 1
T219S	169.7 ± 35	1.03 x 10^4 ± 0.1	17.3 ± 2
L122A	146.3 ± 32	2.67 x 10^4 ± 1	16.8 ± 1
L212A	170.3 ± 50	2.94 x 10^4 ± 0.7	14.7 ± 1
E215A	337.4 ± 50	2.70 x 10^4 ± 0.02	12.9 ± 1
E215D	429.5 ± 24	1.74 x 10^3 ± 0.9	5.5 ± 0.5
E215N	347.3 ± 15	1.62 x 10^3 ± 0.02	12 ± 1

Table 1: Numerical values for the kinetic properties of rAOX TAO wildtype and mutants discussed in the main body of the text. All values are an average of 3 replicates ± SEM.